LBL--15071

DE83 004116

LBL-15071

THE HISS SPECTROMETER AT THE BEVALAC

Douglas E. Greiner

Nuclear Science Division, Lawrence Berkeley Laboratory
University of California, Berkeley, CA 94720

Presented at the International Conference on Nucleus-Nucleus Collisions
Michigan State University, East Lansing, Michigan, September 26-October 1, 1982

This work was supported by the Director, Office of Energy Research, Division of Nuclear Physics of the Office of High Energy and Nuclear Physics of the U.S. Department of Energy under Contract DE-AC03-76SF00098 and National Aeronautics and Space Administration grant number NGR 05-003-513.

THE HISS SPECTROMETER AT THE BEVALAC

Douglas E. GREINER

Nuclear Science Division, Lawrence Berkeley Laboratory
University of California, Berkeley, CA 94720

Abstract: The status of the HISS spectrometer is presented. Preliminary data from multi-particle measurements of the ^{12}C reactions at 1 GeV/n are discussed.

Single particle inclusive measurements have been referred to at this conference as "fishing in the dark" and "a fools' paradise". I have made many measurements of this type and prefer the analogy of the blind men and the elephant. It is hard enough for them to perceive the elephant, much less to take its temperature. However, in the early stages of study, single particle measurements are the necessary first step towards understanding and provide the necessary design parameters for the much more difficult multi-particle experiments.

To show a subset of the motivations behind the building of HISS, I show in fig. 1 a few of the possible reaction types in relativistic heavy ion collisions. Single particle inclusive experiments have shown us that limiting fragmentation is obeyed; this means the physics observed in the projectile frame is equivalent to physics in the target frame and independent of the choice of target material. Thus the reaction mechanism can be studied in the projectile frame where the kinematic focusing and particle laboratory energies make the experimental problems much more tractable. If, for instance, we have resonance formation, be it expected states like ^{8}Be or more exotic particles, they will show up in the invariant mass distributions of the multi-particle measurements. The character of the reaction mechanism in the case of an excitation-decay model will reveal itself through the measurement of the energy and momentum transfer to the excited projectile. These parameters are impossible to observe without an exclusive measurement. In fig. 2 we show the predictions of several models for

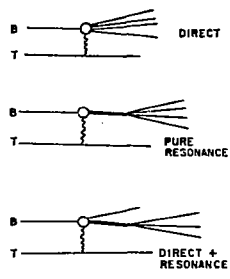

Fig. 1. Some possible reaction sequences.

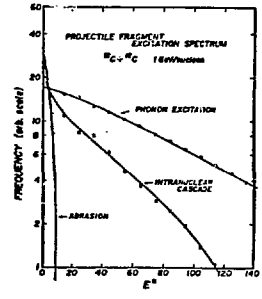

Fig. 2. Predicted interaction energy spectrum.

the excitation energy spectrum in ^{12}C collisions at 1 GeV/n. It is clear that while all three models agree after the decay phase there are major differences in the predictions of the excitation stage. Another type of measurement that motivates the HISS construction is the observation of long-lived states. There has recently been much speculation and some evidence of the existence of abnormal states living as much as several nanoseconds produced as fragments in relativistic heavy ion collisions. Such states, should they decay to charged particles, could be studied as shown in fig. 3. The interaction position is reconstructed allowing measurements of lifetime and mass.

To make such measurements requires first a team of people with the foresight and dedication to spend several years building the necessary apparatus. A list of these people who spent major portions of their full-time effort building HISS is shown in fig. 4. The heart of the HISS spectrometer is the large supercon-

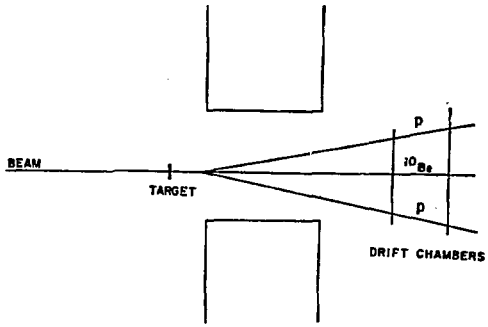

Fig. 3. Decay of a long-lived state.

HEAVY ION SPECTROMETER SYSTEM GROUP

E. PELEAZ	LBL
F. BIESER	LBL
M. BOWINSON	LBL
H. CRAWFORD	UC-SSL
J. ENGELAGE	LSU
J. FLORES	UC-SSL
D. GREINER	LBL
M. JOHNSON	UC DAVIS
P. LINDSTROM	LBL
C. McPARLAND	UC-SSL
J. PORTER	LBL
D. OLSON	LLNL
M. SARA	GSI
R. WADA	LBL

Fig. 4. HISS group members.

ducting magnet (1 m radius, 1 m gap, 3 tesla) shown in fig. 5. The entire facility is designed to allow maximum flexibility in experimental configuration. The magnet rotates, the beam can be steered to enter at a range of angles, the beam stop is movable, and there is a detector platform that moves with the magnet. Triggering and data collection are done in the HISS 2 shack, while the HISS 1 shack houses the VAX 11-780 computer used for on-line diagnostics.

The HISS detector system has evolved in two stages. The phase 1 system shown in fig. 6 was a prototype system built by a large collaboration of experimenters

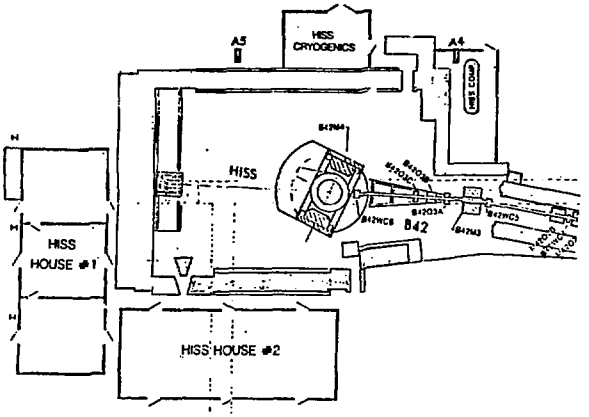

Fig. 5. HISS facility.

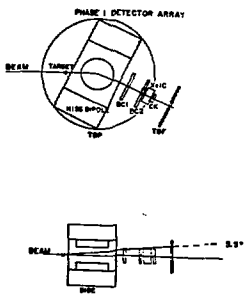

Fig. 6. Phase 1 instrumentation.

to gain early access to data. The phase 1 system consisted of two drift chambers 1 m by 2 m and a time-of-flight wall 2 m by 3 m. The phase 2 configuration (fig. 7) has added a 4 m by 3 m TOF wall, a MUltiple-Sampling-Ionization-Chamber (MUSIC), and will soon include a 2 m by 5 m drift chamber module. The particles are identified by their rigidity, charge, and time of flight. Figure 8 shows the

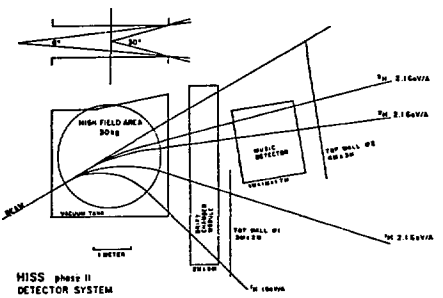

Fig. 7. Phase 2 instrumentation.

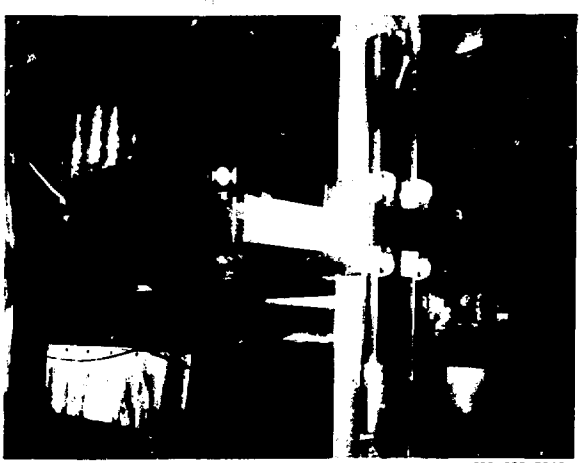

CBB 828-7536

Fig. 8. Magnet gap and mapper.

CBB 828-7538

Fig. 9. HISS cave with TOF walls and MUSIC detector.

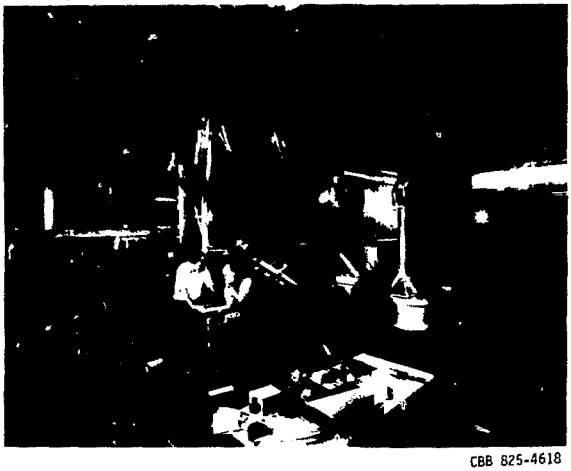

CBB 825-4618

Fig. 10. Magnet vacuum tank and phase 1 drift chambers.

HISS magnet, with its vacuum tank, and, to show the size of the gap, a person working on the magnet mapper apparatus. Figure 9 shows the MUSIC detector, phase 1 and 2 TOF walls. In fig. 10 one can see the phase 1 drift chambers and again the magnet chamber and gap. Another detector, borrowed from Hughes at SLAC is a 49-element NaI detector, to be used to detect neutral particles. A representative cosmic ray muon event in this detector is shown in fig. 11; the

CBB 828-6825

Fig. 11. Muon response of NaI detector.

squares represent the 49 elements, and the energy deposit is indicated by the height and color of the column. A second event, probably a neutron, is shown in fig. 12.

CBB 828-6823

Fig. 12. Neutron response of NaI detector.

The MUSIC detector, similar to the ISIS detector at CERN, is a multiple sampling ionization chamber with a 1 m by 2 m by 1.7 m active volume shown in fig. 13. A photograph of the field cage is fig. 14. The instrument drifts the

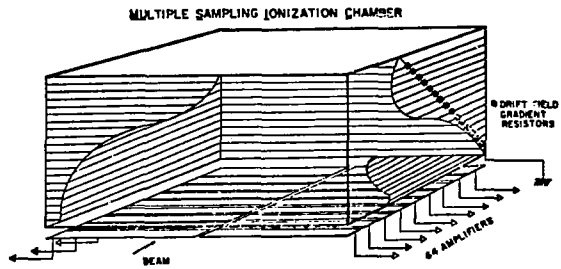

Fig. 13. MUSIC detector configuration.

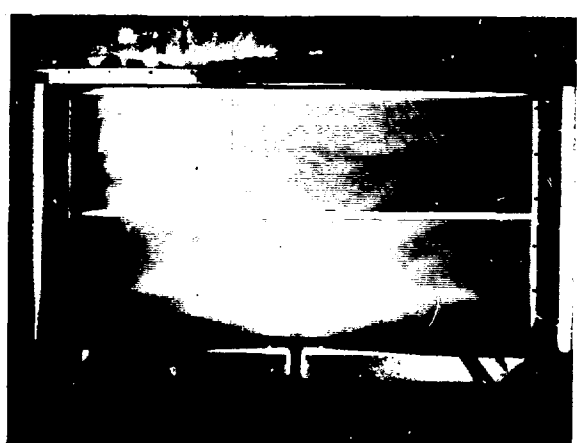

CBB 828-7532

Fig. 14. MUSIC detector field cage.

ionization produced by the particles down to set of 128 anodes as shown in fig. 15. The circuitry used to record the amplitudes is the same as that used in the TPC high energy physics detector built at LBL. The MUSIC detector was built by a collaboration between LBL and UC Davis, Paul Brady representing Davis and Hans Sann for LBL. The MUSIC detector is in its early debug stage this year. We have had a few hours of beam and learned that the design is sound and have devised a satisfactory calibration scheme. Figure 16 shows the pulse heights recorded from a few of the cells for a track made by ^{56}Fe. The two larger signals are due to the fact that every 16th cell is three times the usual 2-cm width to allow extension of the dynamic range to as low as charge 6. A calibration pulser signal is included in fig. 17; the correlations in pulse height between pulser and signal indicate the necessity to include calibration information with each event. We expect the MUSIC detector to be ready for experimenters within the next year.

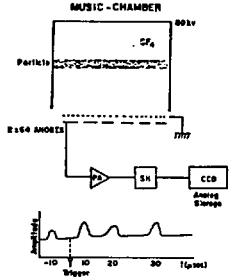

Fig. 15. MUSIC signal processing.

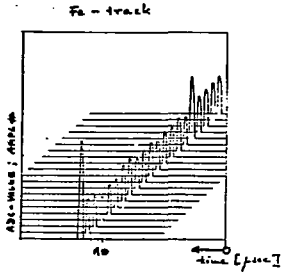

Fig. 16. MUSIC response to ^{56}Fe beam.

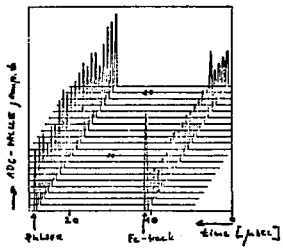

Fig. 17. MUSIC response to ^{56}Fe beam with pulser.

Five experiments were approved for the first round of HISS running, shown on fig. 18. The running time this year allowed six weekends, which were used to complete the INS high momentum transfer experiment and the ^{12}C multi-particle final states experiment by the HISS group. Data were also taken by Igo et al. on p-p correlations in mid-rapidity and tests of the MUSIC detector with beams of ^{56}Fe and ^{40}Ar. These runs, using three experimental configurations in less than three months, show that the flexibility built into HISS is paying off.

The INS experiment was the first experiment completed on HISS. The goals of this experiment are shown on fig. 19. The configuration of this experiment, shown in fig. 20, shows how the INS group has augmented the common detectors with a second spectrometer arm inside the magnet to measure high momentum transfer correlations. In this case the user group invested a large amount of effort to augment the common detectors. The p-p correlation experiment by Igo et al., the goals of which are shown in fig. 21, illustrates the opposite extreme. Their experimental configuration is shown in fig. 22; the setup can actually be achieved by moving the common detectors and mounting a few simple detectors in the beam line.

HISS PHASE I EXPERIMENTS

COULOMB DISSOCIATION OF $^{16,18}O$—LLL, SSL, LBL

GOALS: EXCITATION OF GIANT RESONANCES IN $^{16,18}O$ DECAY

INVARIANT MASS SPECTRA FROM ^{12}C—LSU, SSL, MCD, ATC, LBL

GOALS: EXCITATION SPECTRA FROM EXCLUSIVE MODES
SEARCH FOR STRUCTURE IN INVARIANT MASS SPECTRA

FRAGMENTATION OF ^{56}Fe—SSL, BNL, LBL

GOALS: SEARCH FOR COLLECTIVE EFFECTS EVIDENCED BY STRUCTURE IN INVARIANT MASS SPECTRA

MEASUREMENTS OF LARGE P_T FRAGMENTS—IAS, LBL

GOALS: STUDY COLLECTIVE EFFECTS NEAR KINEMATIC LIMITS AND THE ASSOCIATED MULTIPLICITIES

TWO PARTICLE CORRELATIONS AT SMALL ΔQ—OCLU, MCD, LBL

GOALS: USE SECOND ORDER INTERFERENCE BETWEEN IDENTICAL PARTICLES TO DETERMINE INTERACTION VOLUME AND TIME

Fig. 18. Phase 1 experiments.

GOAL OF THE EXPERIMENT

Study of High Energy-Density Created in Relativistic Nuclear Collisions

(1) How does the total energy of the reaction concentrate to high P_T particles ?
Exponential decrease of inclusive cross section persists at high P_T ?

(2) How does the concentrated energy dissipate in the nucleus ?

recoil-like mode	high P_T - low P_T correlation
jet-like mode	high P_T - high P_T correlation

Fig. 19. INS experimental goals.

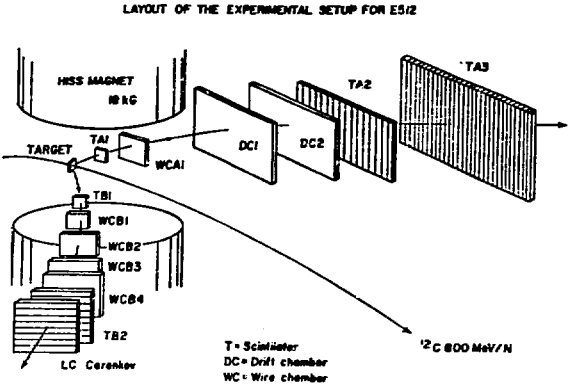

Fig. 20. INS experimental setup.

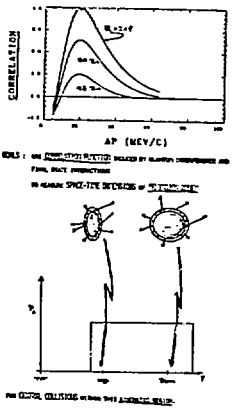

Fig. 21. Igo et al. experimental goals.

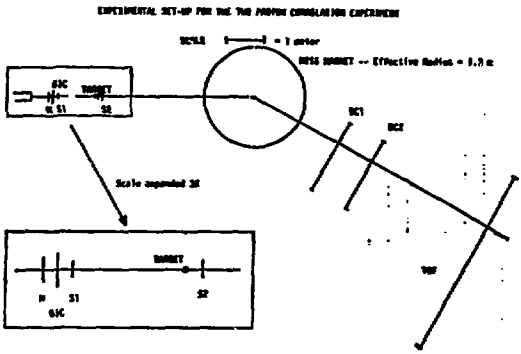

Fig. 22. Igo et al. experimental setup.

I would now like to present some preliminary data from the ^{12}C exclusive state experiment done by the HISS group two months ago. The experiment was designed to be run at 2.1 GeV/n beam energy, but unfortunately the run was made at 1 GeV/n because of budget constraints, which would not allow high energy operation of the Bevalac at that time. The lower beam energy caused a much smaller rate of fully reconstructable events caused by the reduced kinematic focusing at the lower energy.

The experimental configuration is shown in fig. 23; the trigger was a beam particle that gave a TOF start pulse in the upstream scintillator, TOF 1, and a pulse height corresponding to ^{12}C in the E counter by the target and no signal of z = 6 in the DS counter in front of the TOF wall. Thus the trigger was carbon in, no carbon out. The trajectory of the incoming beam was recorded by the drift chambers DC3 and DC4 near the target. The fragments were detected in drift chambers DC1 and DC2 and the TOF wall downstream of the target. The raw charge signal in the TOF wall is shown in fig. 24. These data illustrate the unity and interdependence of the detectors in several ways; the z = 3 to 4 region does not show good charge resolution by the wall alone because the cases where there are two alpha particles in a single slat causes broadening. Such events are a result of ^{8}Be decay and require the information from the drift chambers to correct the data. Another case is the events at z = 0.5; these events are delta rays, which are made in the space between the drift chambers and the TOF wall. Such events are rejected when a valid trajectory is required in the drift chambers and magnet as shown in fig. 25. The rigidity is determined using the trajectories from the drift chambers a table lookup routine for ray tracing in the magnetic field. The separation in rigidity versus TOF wall slat number shown in fig. 26 shows the first glimmer of physics content, namely, that there are not large numbers of z = 1 particles other than the expected 1H, 2H and 3H. In fig. 27 we have used the TOF signal to produce the mass distribution of the z = 1 particles. At this time, with the rough field map we have, the mass resolution is around 100 MeV.

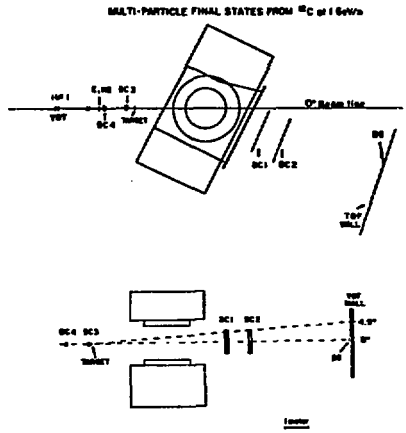

Fig. 23. HISS group experimental setup.

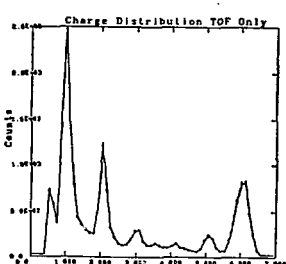

Fig. 24. Charge distribution in TOF wall.

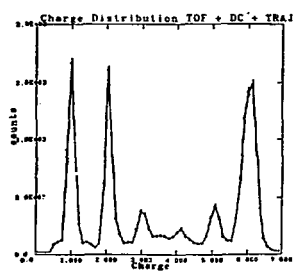

Fig. 25. Charge distribution TOF + drift chamber trajectory.

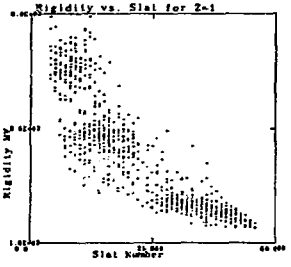

Fig. 26. Rigidity versus TOF slat number, z = 1.

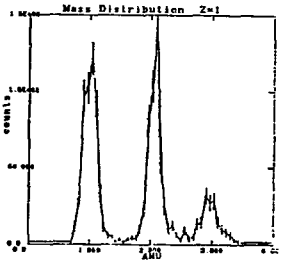

Fig. 27. Mass distribution z = 1.

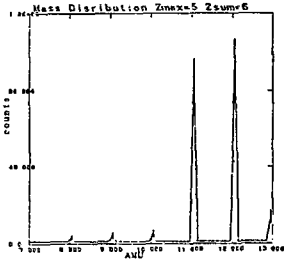

Fig. 28. Mass distribution for events with maximum charge = 5 and charge sum = 6.

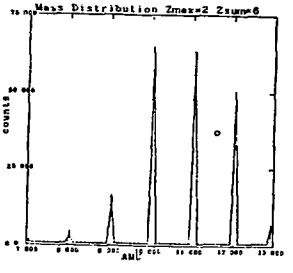

Fig. 29. Mass distribution for events with maximum charge = 2 and charge sum = 6.

The fully reconstructable events we need to measure the excitation energy distribution require that there be sufficient signal in the reaction channels that do not contain neutrons. Figure 28 shows how well we are doing in this respect; plotted is the mass distribution when the event contains a z = 5 particle and the total charge in the event is six. From the plot we see that about 50% of the time we miss a single neutron. The situation should change as we look at higher multiplicity events as shown in fig. 29 where we cannot reconstruct about 70% of the events because of missing neutrons.

The primary goal of this experiment is the measurement of the excitation spectrum that is the energy transferred to the excited ^{12}C projectile. This quantity is constructed by calculating the invariant mass of the fully reconstructable events and subtracting the mass of the unexcited incoming beam. In fig. 30 we see for the first time this excitation spectrum. There are several interesting points: the spectrum does not peak at zero excitation, it falls off close to that predicted by the cascade prediction shown in fig. 2, and there is a long tail extending up to very high excitations in the hundreds of MeV region. Because these data are preliminary there are several warnings I should make about possible sources of bias: first, because of the small acceptance of the detectors at 1 GeV/n, the spectrum is probably biased towards low excitation events; another bias in the same direction is the fact that this spectrum is dominated by two body finals states and we have not yet analyzed the six body events. The reason I show these data at this time is to demonstrate the power of the method and the fact that we are well on the way to achieving our goal. The fact that we can now measure in an unambiguous way the total energy transfer in a reaction means we can now select very small or very large excitation events and study them in detail.

The second advantage of these multi-particle measurements is to allow measurement of the interaction position to search for long-lived states. This involves the fitting of the topology of an event allowing the interaction position to be a free variable. So far we have only done this in the z coordinate, which is unaffected by the magnetic field. When we have an accurate field map we will do it in the x and y coordinates also; however, the current results are of interest and demonstrate the progress and the method. In fig. 31 we plot the interaction position obtained by fitting the two and three particle events to a topology that makes no assumption about the position of the interaction; the interaction position in cm is the abscissa. The center of the magnet is 0.0 and the drift chamber position is +275 cm. The distribution peaks at the target position of -330 cm with a resolution of about 50 cm. This resolution corresponds to about 0.1 mr accuracy in the angular measurements. To search for

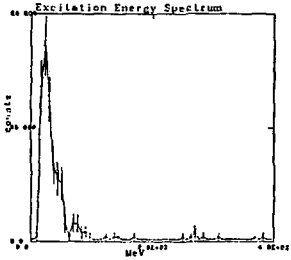

Fig. 30. Excitation energy spectrum.

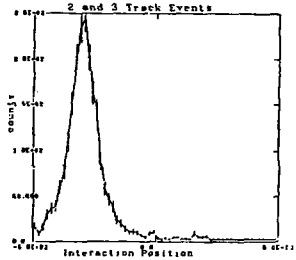

Fig. 31. 2 and 3 track interaction positions.

long-lived states we apply the following analysis: long-lived states should be revealed through their mass in an invariant mass plot. At this stage of the analysis we can demonstrate the method and get a first rough look by separating the data set into two samples, those events that appear to originate at or before the target and those that come from downstream of the target. Thus we are enriching the downstream sample with the possible long-lived states. We then compare the invariant mass distributions of the two samples in figs. 32 and 33.

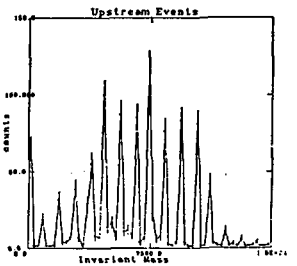

Fig. 32. Invariant mass distribution for upstream event sample.

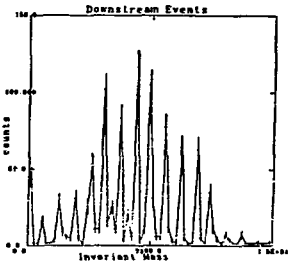

Fig. 33. Invariant mass distribution for downstream event sample.

In these figures we see peaks at the masses of the stable particles observed and the same within statistics for the two samples. There is a hint of a difference between masses 5-6 and 6-7. This is most probably due to the current state of the analysis and not a real signal. The method is demonstrated; we do not understand everything we see right now, but we will.

This work was supported by the Director, Office of Energy Research, Division of Nuclear Physics of the Office of High Energy and Nuclear Physics of the U.S. Department of Energy under Contract DE-AC03-76SF00098 and National Aeronautics and Space Administration grant number NGR 05-003-513.